Determinants of Cooperativity and Site Selectivity in Human Ileal Bile Acid Binding Protein

Orsolya Toke,* John D. Monsey, Gregory T. DeKoster, Gregory P. Tochtrop, Changguo Tang, and David P. Cistola*

Department of Biochemistry and Molecular Biophysics, Washington University School of Medicine, St. Louis, Missouri 63110

Received September 4, 2005; Revised Manuscript Received November 22, 2005

ABSTRACT: Human ileal bile acid binding protein (I-BABP) is a member of the family of intracellular lipid-binding proteins and is thought to play a role in the enterohepatic circulation of bile salts. Our group has previously shown that human I-BABP binds two molecules of glycocholate (GCA) with low intrinsic affinity but an extraordinary high degree of positive cooperativity. Besides the strong positive cooperativity, human I-BABP exhibits a high degree of site selectivity in its interactions with GCA and glycochenodeoxycholate (GCDA), the two major bile salts in humans. In this study, on the basis of our first generation nuclear magnetic resonance (NMR) structure of the ternary complex of human I-BABP with GCA and GCDA, we introduced single-residue mutations at certain key positions in the binding pocket that might disrupt a hydrogen-bonding network, a likely way of energetic communication between the two sites. Macroscopic binding parameters were determined using isothermal titration calorimetry, and site selectivity was monitored by NMR spectroscopy of isotopically enriched bile salts. According to our results, cooperativity and site selectivity are not linked in human I-BABP. While cooperativity is governed by a subtle interplay of entropic and enthalpic contributions, site selectivity appears to be determined by more localized enthalpic effects. Possible communication pathways between the two binding sites are discussed.

Human ileal bile acid binding protein (I-BABP)[1] belongs to the family of intracellular lipid-binding proteins, a group of small, approximately 15-kDa proteins that bind fatty acids, retinoids, cholesterol, and bile salts (*1*, *2*). Human I-BABP is abundantly expressed in the absorptive enterocytes of the distal small intestine (*3*−*5*) and is thought to play a role in the transcellular trafficking and enterohepatic circulation of bile salts (*6*).

Our group has previously shown that human I-BABP binds two molecules of glycocholate (GCA), the physiologically most abundant bile salt, with low intrinsic affinity but a remarkable high degree of positive cooperativity (*7*). Furthermore, calorimetric analysis of the binding of nine physiologically relevant bile acid derivatives in their conjugated and unconjugated forms as well as a series of side-chain-extended bile salts has indicated that cooperativity in bile salt-I-BABP recognition is governed by the pattern of steroid ring hydroxylation, rather than the presence and type of side-chain conjugation (*8*). In addition to the strong positive cooperativity observed for the derivatives of cholic acid, human I-BABP has been found to exhibit a high degree of site selectivity in its interactions with GCA and glycochenodeoxycholate (GCDA) (Figure 1), the two primary bile salts in humans (*9*). Although the two bile salts differ only in a single hydroxyl group at position C-12 of their steroid ring system, when the protein is incubated with a mixture of the two bile salts, GCA binds nearly exclusively to one site, while GCDA binds nearly exclusively to the other site. [When human I-BABP is incubated with GCA or GCDA *only*, both binding sites are occupied as observed by nuclear magnetic resonance (NMR) spectroscopy.]

The reasons for the asymmetry displayed by I-BABP in its interactions with GCA and GCDA are not yet clear. One possibility is that site selectivity arises from differences in cooperativity. Alternatively, site selectivity may be the result of a number of highly specific local interactions between bile salts and protein side chains in a manner less dependent on the cooperative nature of the system.

The goal of the present study was to gain more insight into the structural correlates of cooperativity and site selectivity in human I-BABP. On the basis of NMR-derived interproton distance restraints between bound bile salts and wild-type (WT) I-BABP, in combination with a homology model of the protein structure, we developed a structural model of the ternary complex of human I-BABP with GCA and GCDA (1:1.5:1.5) that provided us with information on the location and orientation of the ligands in the binding cavity. (The full 3D NMR structure of the protein will be described in a subsequent paper.) On the basis of this

* To whom correspondence should be addressed: Department of Biochemistry and Molecular Biophysics, Washington University School of Medicine, 660 South Euclid Avenue, Campus Box 8231, St. Louis, MO 63110. Telephone: 314-362-4382. Fax: 314-362-7183. E-mail: cistola@cosine.wustl.edu (D.P.C.); Institute of Structural Chemistry, Chemical Research Center, Hungarian Academy of Sciences, Pusztaszeri út 59−67. H-1025 Budapest, Hungary. Telephone: 36-1-438-4141/289. Fax: 36-1-325-7554. E-mail: toke@chemres.hu (O.T.).

[1] Abbreviations: GCA, glycocholic acid; GCDA, glycochenodeoxycholic acid; HSQC, heteronuclear single-quantum coherence; ITC, isothermal titration calorimetry; I-BABP, ileal bile acid binding protein; NMR, nuclear magnetic resonance; NOESY, nuclear Overhauser and exchange spectroscopy; WT, wild type.

10.1021/bi051781p CCC: $33.50
Published on Web 12/24/2005

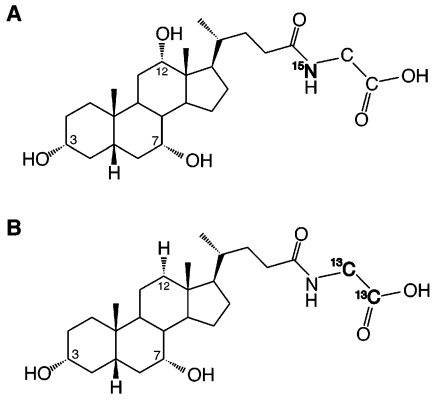

FIGURE 1: Chemical structures of glycocholic acid (GCA) (A) and glycochenodeoxycholic acid (GCDA) (B). The positions of the ^{15}N (GCA) and ^{13}C (GCDA) labels used in the site-selectivity experiments are shown in bold.

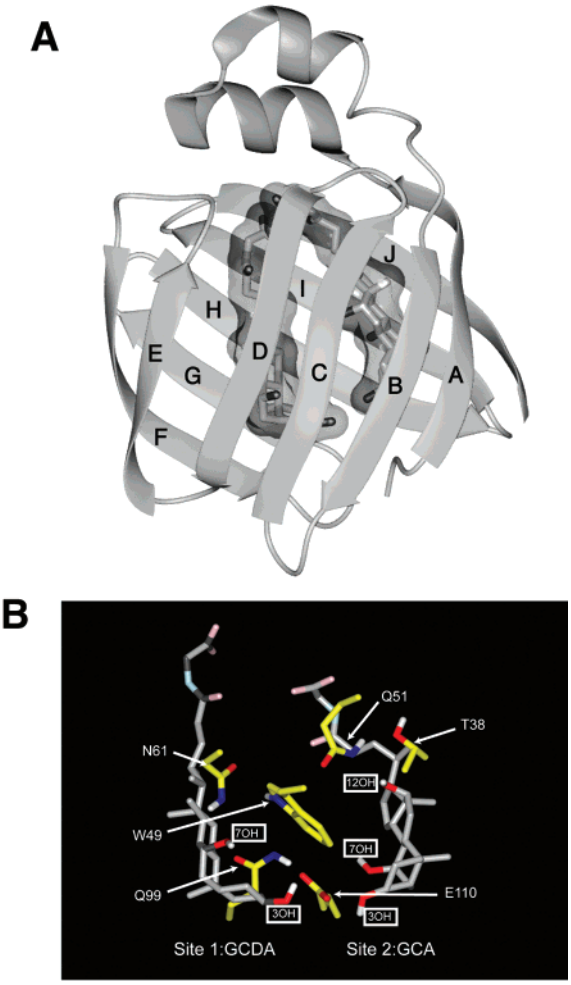

FIGURE 2: Homology model of human I-BABP with GCA and GCDA docked by restrained energy minimization. (A) Human I-BABP binds two molecules of bile salts in an enclosed cavity surrounded by two antiparallel β sheets. (B) Binding pocket of human I-BABP. The two binding sites were identified by NOE-derived bile salt−protein distance restraints in the ternary complex of human I-BABP with GCA and GCDA (1:1.5:1.5).

structural model, we introduced six single-residue mutations at certain key positions in the binding pocket (Figure 2) that might disrupt a hydrogen-bonding network, a likely way of energetic communication between the two sites. Macroscopic binding parameters were determined using isothermal titration calorimetry (ITC), and site selectivity was monitored by NMR spectroscopy of isotopically enriched (^{13}C and/or ^{15}N) bile salts (Figure 1).

MATERIALS AND METHODS

Protein Biosynthesis and Purification. Mutagenic primers were obtained from Integrated DNA Technologies (Coralville, IA).

Site-directed mutagenesis was carried out using overlap extension polymerase chain reaction (*10*−*11*). The *Escherichia coli* strain, MG1655, transformed with the mutated pMON-hIBABP construct, was incubated overnight in 80 mL of TB media containing 100 μg/mL ampicillin and then divided and transferred into six 2-L flasks, containing 700 mL of TB media each. Protein expression, under the control of the recA promoter, was induced by the addition of 7 mL of 10 mg/mL nalidixic acid to the growing culture at OD_{600} = 0.5−0.6, and cells were allowed to grow 3−4 h more, harvested, and frozen at −70 °C. The expression of uniformly $^{13}C/^{15}N$-enriched protein followed a two-stage strategy designed to achieve an optimal balance between cell growth and isotope utilization (*12*), the details of which will be given in a subsequent paper. The cell pellet was thawed in 20 mL of 20 mM Tris-HCl at pH 8.0 and 5 mM EDTA, containing a broad-spectrum protease inhibitor mixture (Roche Molecular Biochemicals). The protein was released from either (1) partially lysed cells by using a freeze−thaw protocol described elsewhere (*13*) (WT, W49Y, Q51A, and N61A) or (2) by processing the cell suspension through french-press 3−4 subsequent times (Q99A, E110A, and T38A). The homogenized cell suspension was subjected to centrifugation at 4 °C, 15000*g* for 30 min. Because some mutant proteins appeared to be produced as inclusion bodies, both the supernatant and the pellet were analyzed by SDS−PAGE to determine which fraction would contain most of the mutant protein. If the majority of the protein was present in the supernatant, method 1 (see below) was employed for further purification. If more than 50% of the protein appeared to form inclusion bodies, method 2 was employed.

Method 1: Purification of hI-BABP Derivatives from Supernatant Solution (WT, W49Y, Q51A, and Q99A). The clarified supernatant was chromatographed on a 25 × 5 cm column of Q-Sepharose Fast Flow. Dialysis was carried out against multiple changes of 10 mM Tris at pH 8.2 and 0.05% NaN_3 at 4 °C, until the A_{260}/A_{280} absorbance ratio decreased below 0.7. The protein solution was then subjected to another ion-exchange chromatograpy on Q-Sepharose Fast Flow. Delipidation was achieved by passing the protein solution over a column of lipophilic Sephadex type VI (Sigma product number H-6258) pre-equilibrated with 20 mM potassium phosphate, 135 mM KCl, 10 mM NaCl, and 0.05% NaN_3 (pH 7.2), at 37 °C. Protein purity, as assessed by overloaded Coomassie-stained SDS−PAGE gels, was >98%.

Method 2: Recovery of hI-BABP Derivatives from Inclusion Bodies (N61A, E110A, and T38A). The pellet, containing the inclusion bodies, was washed 5−6 times with 20 mM Tris-HCl and 0.25 mM EDTA at pH 8.0 (buffer A), centrifuged for 30 min at 4 °C at 10000*g*, and dissolved in 15 mL of 6 M Gdn in buffer A. The following day the insoluble material was removed by centrifugation. The unfolded protein was renatured by diluting 100-fold into

buffer A and then concentrated to about 100 mL using a YM-3 membrane. Aggregates were removed by centrifugation (10000*g*, 30 min). After thorough dialysis against buffer A, mutant proteins were over 98% homogeneous as determined by the Coomassie Blue-stained SDS−PAGE gel. Because these proteins formed aggregates at 37 °C, delipidation was carried out at room temperature.

Protein concentrations were determined by absorbance at 280 nm. Extinction coefficients corresponding to a 1 mg/mL solution of the appropriate mutant human I-BABP in water were obtained using composition analysis according to Pace et al. (*14*) and were as follows: WT, 0.91; W49Y, 0.497; Q51A, 0.849; N61A, 0.851; Q99A, 0.876; E110A, 0.869; and T38A, 0.885 A mg^{-1} mL^{-1}.

NMR Sample Preparation. [1′,2′-$^{13}C_2$]- and [^{15}N]-labeled bile salts were synthesized via peptide coupling of [1′,2′-$^{13}C_2$]-glycine or ^{15}N-enriched glycine (Cambridge Isotope Laboratories) to unconjugated bile salts by the method of Tserng et al. (*15*). Unenriched bile salts were obtained from Sigma. The isotopically enriched and unenriched bile salts were dissolved in tetrahydrofuran. The concentration of stock solutions was determined by measuring the dry weight of a 10 μL aliquot on a Perkin−Elmer AD-4 microbalance. Gastight Hamilton syringes were used to aliquot the appropriate amounts of the stock solutions, and the solvent was evaporated under a stream of N_2. The bile salt was solubilized with 1.1 equivalent of 1 M KOH and brought up to a volume of 60 μL in a buffer containing 20 mM potassium phosphate, 135 mM KCl, 10 mM NaCl, and 0.05% NaN_3 at pH 7.2. The solution was lyophilized overnight, and then 540 μL of protein solution (0.66−0.9 mM) in the same buffer was added, followed by the addition of 60 μL of D_2O.

NMR Data Collection. Multidimensional NMR spectra were accumulated using Varian Unity Inova 500 and 600 three-channel NMR spectrometers equipped with a Nalorac 5 mm indirect triple resonance *z*-axis gradient probe. Processing and analysis of NMR spectra were performed off-line using Sun and Silicon Graphics Unix workstations. For initial spectral processing, VNMR, FELIX, and NMR PIPE were used. For subsequent spectral analysis, computer-assisted spin-system analysis, resonance assignment, and restraint derivation, FELIX-ASSIGN was used. The resonance assignment strategy utilized uniformly [U-^{13}C/^{15}N]-enriched WT human I-BABP and a series of 3D gradient-enhanced triple-resonance experiments (*16*−*25*). The backbone assignments were established using 3D g-HNCACB (*16*−*18*), g-CBCACONNH (*19*), g-HNCO (*17*−*18*, *20*−*21*), and g-CBCACOCAHA (*22*). Subsequent side-chain assignments involved 3D CC-TOCSY-NNH (*23*), HCC-TOCSY-NNH (*23*), and g-HCCH-TOCSY (*24*). Aromatic assignments were established by a series of 2D experiments (*25*) that exploit scalar couplings between the aliphatic H_β and the aromatic C_γ and then subsequently between the aromatic C_γ and the aromatic ring protons [2D CG(CB)HB, 2D CG(CD)HD, and 2D CG(CDCE)HE]. The NOE-derived distance restraints between ^{13}C- or ^{15}N-enriched bile salts and human I-BABP were generated using 2D gradient-enhanced versions of the ^{13}C- and ^{15}N-edited nuclear Overhauser and exchange spectroscopy (NOESY) experiments (*26*−*27*).

In the site-selectivity experiments, gradient- and sensitivity-enhanced ^{1}H/^{15}N heteronuclear correlation spectra (^{15}N-HSQC) on ^{15}N-labaled bile salts complexed with various unlabeled I-BABP derivatives were collected using the pulse sequence of Kay and co-workers (*28*). ^{15}N-HSQC spectra were acquired with a ^{1}H spectral width of 6500 Hz and 2048 complex points, zero-filled to a total of 4096 points. Gradient-enhanced ^{1}H/^{13}C heteronuclear correlation spectra (^{13}C-HSQC) (*29*) on ^{13}C-labeled bile salts complexed with various unlabeled I-BABP derivatives were acquired with a ^{1}H spectral width of 6500 Hz and 1024 complex points, zero-filled to a total of 2048. In the ^{13}C dimension, 512 hypercomplex increments were collected and zero-filled to a total of 1024 points. Gaussian- and exponential-weighting functions were applied in the F2 dimension, while the indirectly detected dimensions were Gaussian-weighed only.

Development of a First Generation Structural Model of the Doubly Ligated Human I-BABP Complex. The secondary structure of human I-BABP was determined using NMR chemical shifts (*30*). Given the 76% sequence identity and the high degree of topological conservation between human and porcine I-BABP, a homology model for human I-BABP was constructed on the basis of coordinates of the NMR structure of porcine I-BABP (*31*). NOE-derived interproton distance restraints between the ends of the bound bile salt molecules and the protein were used to orient the two bile salts in the binding cavity. The model was subjected to several energy-minimization and simulated-annealing steps using the Discover module of Insight II (Molecular Simulations, San Diego, CA).

Equilibrium Unfolding Monitored by Fluorescence Spectroscopy. Ultrapure urea was the product of United States Biomedical. The concentration of urea was determined by the refractive index at 25 °C (*32*). WT and mutant human I-BABP were unfolded at urea concentrations from 0 to 8.0 M in 20 mM potassium phosphate, 135 mM KCl, 10 mM NaCl, and 0.05% NaN_3 at pH 7.2 and equilibrated at room temperature for 20 h. The fluorescence emission spectrum was measured on a PTI fluorimeter (Photon Technology International, Inc.) using 2 μM protein solution at 25 °C. WT, T38A, Q51A, N61A, Q99A, and E110A hI-BABP were excited at 285 nm, and the fluorescence emission was recorded at 370 nm. W49Y hI-BABP was excited at 275 nm, and the fluorescence emission was monitored at 300 nm. The parameters indicative of the energetic stability of the proteins were calculated using the linear extrapolation method from Santoro and Bolen (*33*).

Isothermal Titration Calorimetry (ITC). Bile salts were obtained from Sigma and were dissolved in a buffer containing 20 mM potassium phosphate, 135 mM KCl, 10 mM NaCl, and 0.05% NaN_3 at pH 7.2. The protein was dialyzed into the same buffer. The calorimetry experiments were performed using a Microcal OMEGA differential titration calorimeter. A total of 15 injections of 4 μL aliquots were followed by 35 injections of 7 μL aliquots of 6.5 mM bile salt into the reaction cell containing 1.33 mL of 0.2 mM mutant human I-BABP, unless noted otherwise. Titrations were carried out at 25 °C. Each titration series was repeated 3 or 4 times. The heats of injection were corrected for the heat of dilution of the ligand into the buffer and normalized to the amount of bile salt injected. The integrated peak intensities were fit to a stepwise binding model shown

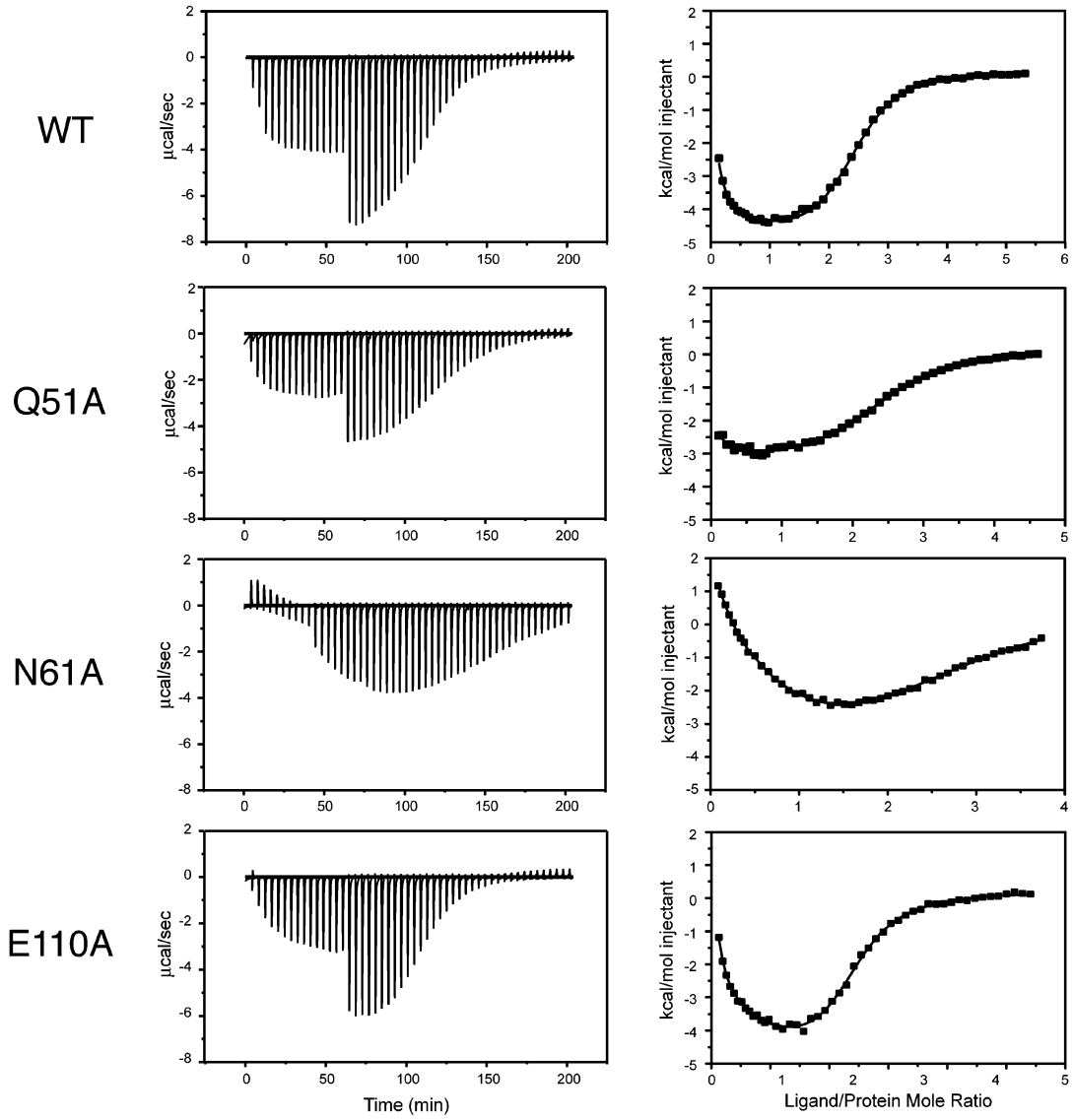

FIGURE 3: ITC results for GCA binding to human I-BABP derivatives. The raw data, as injection profiles, as well as least-squares fitted isotherms are shown for WT human I-BABP and mutants Q51A, N61A, and E110A. The curve through the points represents a least-squares fit of the raw data using the stepwise binding model defined in eq 1. The discontinuity at an *x*-axis value of approximately 60 min in the injection profiles represents a change in the injection volume from 4 to 7 μL.

schematically as

$$P \overset{L,\ K_1^{obs}}{\rightleftharpoons} PL \overset{L,\ K_2^{obs}}{\rightleftharpoons} PL_2 \quad (1)$$

using Bayesian analysis as described elsewhere (*34*).

RESULTS

Titration Calorimetry Experiments To Determine Bile Acid Binding Parameters. The six single-residue mutations that we investigated in the binding pocket of human I-BABP are shown in Figure 2B. Injection profiles and binding isotherms for the interactions of WT, Q51A, N61A, and E110A human I-BABP with GCA and GCDA are shown in Figures 3 and 4. Curves of similar characteristics were obtained for T38A, W49Y, and Q99A human I-BABP (data not shown). All mutants exhibited biphasic binding profiles, similar to the ones that we observed for WT protein. To quantitate the affinities, free energies, enthalpies, and entropies for bile salt binding, ITC data sets were fit to the stepwise binding model shown in eq 1 using Bayesian analysis. Initial values for the parameter search were obtained from nonlinear least-squares fitting. As we described earlier (*8*), Bayesian analysis circumvents the problem of underestimating the parameter space consistent with the data, a phenomenon particularly prevalent in nonlinear least-squares analysis of systems with positive cooperativity. The dissociation constants and stepwise binding enthalpies together with the calculated Hill coefficients, a commonly used measuring stick for macroscopic cooperativity, are listed in Tables 1 and 2 for the binding of GCA and GCDA, respectively. This latter parameter adopts a value of 1 for a noncooperative system and a maximum value of 2 for a two-site system with infinite positive cooperativity. Bayesian analysis of the probability distribution for the fitted stepwise dissociation constants for the binding of GCA and GCDA to various human I-BABP derivatives is shown in Figure 5.

Among the engineered mutations, N61A resulted in the most severe loss of macroscopic positive cooperativity with Hill coefficients of 1.2 and 0.5 for GCA and GCDA,

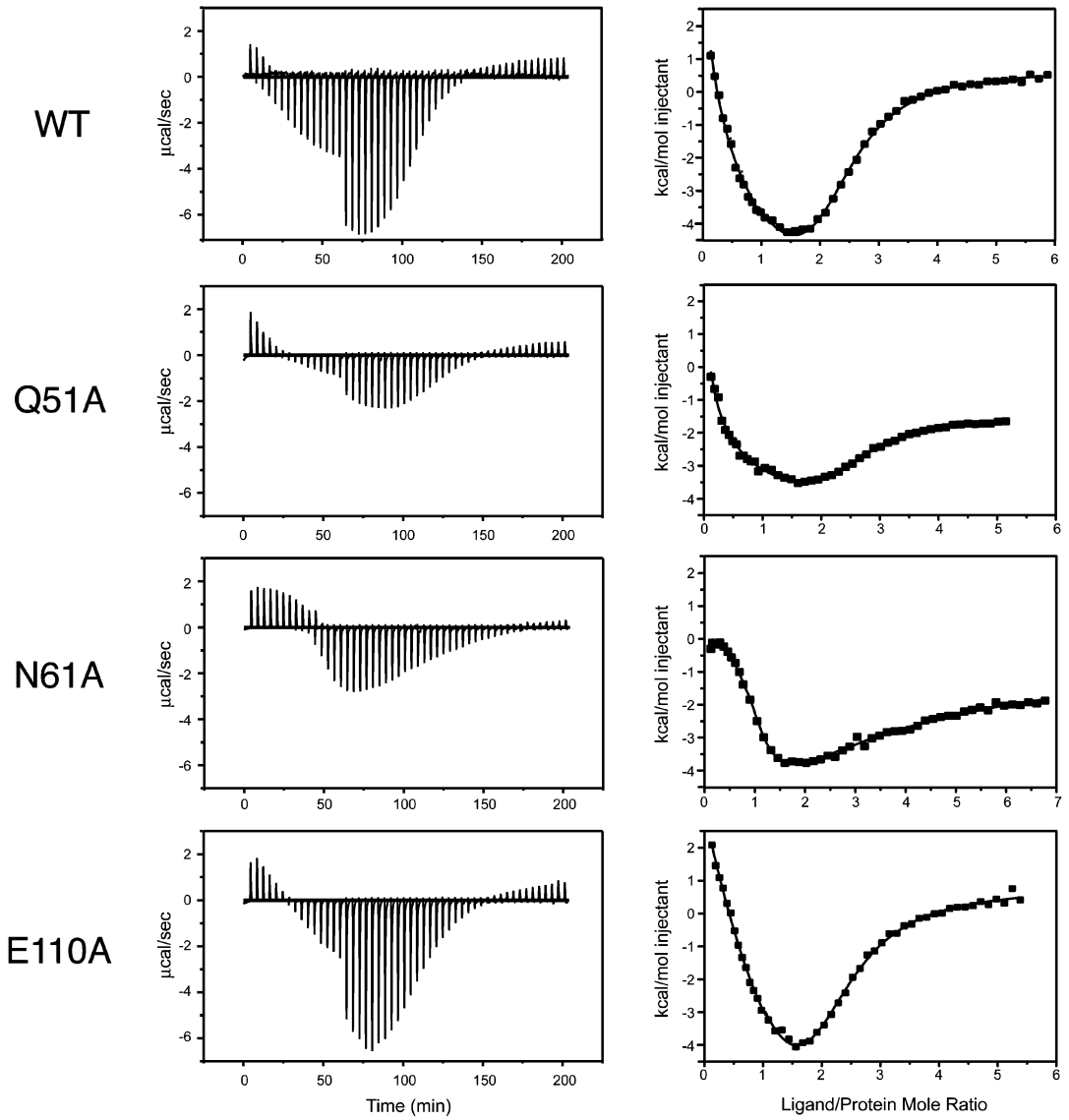

FIGURE 4: ITC results for GCDA binding to human I-BABP derivatives. The raw data, as injection profiles, as well as least-squares fitted isotherms are shown for WT human I-BABP and mutants Q51A, N61A, and E110A. The curve through the points represents a least-squares fit of the raw data using the stepwise binding model defined in eq 1. The discontinuity at an *x*-axis value of approximately 60 min in the injection profiles represents a change in the injection volume from 4 to 7 μL.

Table 1: Stepwise Binding Parameters for the Interaction of Investigated Human I-BABP Derivatives with GCA at 25 °C

hI-BABP type	n_H[a]	$K_{d_1}^{obs}$ (μM)	$K_{d_2}^{obs}$ (μM)	$\Delta H°_1^{obs}$ (kcal/mol)	$\Delta H°_2^{obs}$ (kcal/mol)	$T\Delta S_1^{obs}$ (kcal/mol)	$T\Delta S_2^{obs}$ (kcal/mol)
wild type[b]	1.82 ± 0.03	490 ± 110	4.3 ± 1.2	3.3 ± 2.9	−12 ± 0.4	7.8 ± 2.9	−4.7 ± 0.4
wild type[c]	1.84 ± 0.02	748 ± 170	5.9 ± 1.1	2.4 ± 1.5	−11.1 ± 0.1	6.7 ± 1.5	−4.0 ± 0.1
T38A	1.73 ± 0.02	225 ± 40	5.4 ± 0.6	−1.7 ± 0.3	−10.2 ± 0.1	3.3 ± 1.2	−3.0 ± 0.1
W49Y	1.54 ± 0.03	477 ± 50	42 ± 6	−1.0 ± 0.3	−11.3 ± 0.5	3.5 ± 0.3	−5.3 ± 0.1
Q51A	1.73 ± 0.02	773 ± 110	19 ± 3	−3.3 ± 0.1	−8.3 ± 0.1	0.9 ± 1.0	−1.8 ± 0.1
N61A	1.20 ± 0.04	497 ± 40	220 ± 30	0.7 ± 0.3	−17.6 ± 2	5.2 ± 0.3	−12.6 ± 0.5
Q99A	1.80 ± 0.02	846 ± 110	9.9 ± 1.2	5.9 ± 1.2	−11.6 ± 0.1	10.1 ± 0.1	−4.8 ± 0.1
E110A	1.50 ± 0.01	183 ± 10	21 ± 1	0.2 ± 0.1	−10.8 ± 2	4.9 ± 0.3	−4.4 ± 2

[a] The Hill coefficient is related to the stepwise binding parameters as follows: $n_H = 2/[1 + (K_{d_2}^{obs}/K_{d_1}^{obs})^{1/2}]$. [b] Tochtrop et al. (2003) *Biochemistry 42*, 11561−11567. [c] This study.

respectively (versus 1.82 and 1.34 obtained for WT human I-BABP). Mutant Q99A exhibited similarly diminished cooperativity in the binding of GCDA. Mutations at E110 and W49 resulted in moderate but significant losses in binding cooperativity.

As it is revealed by the products of $K_{d_1}^{obs}$ and $K_{d_2}^{obs}$, overall binding affinities in the mutant proteins range from about 25-fold weaker (N61A for GCA) to about 2-fold stronger (T38A for GCDA) than in WT human I-BABP. These differences largely arise from the second binding step and are reflections of the changes in macroscopic binding cooperativity.

For most human I-BABP derivatives (including WT protein), the first binding step has a large entropically

Table 2: Stepwise Binding Parameters for the Interaction of Investigated Human I-BABP Derivatives with GCDA at 25 °C

hI-BABP type	n_H[a]	$K_{d_1}^{obs}$ (μM)	$K_{d_2}^{obs}$ (μM)	$\Delta H^\circ_1{}^{obs}$ (kcal/mol)	$\Delta H^\circ_2{}^{obs}$ (kcal/mol)	$T\Delta S_1^{obs}$ (kcal/mol)	$T\Delta S_2^{obs}$ (kcal/mol)
wild type[b]	1.34 ± 0.04	62 ± 6	15 ± 2	2.8 ± 5.0	−12.0 ± 0.3	8.5 ± 5.0	−5.4 ± 0.3
wild type[c]	1.33 ± 0.01	103 ± 5	26 ± 1	3.0 ± 0.2	−12.3 ± 0.1	8.4 ± 0.2	−6.0 ± 0.1
T38A	1.44 ± 0.01	62 ± 2	9.5 ± 0.3	1.7 ± 0.1	−10.8 ± 0.1	7.4 ± 0.1	−3.9 ± 0.1
W49Y	1.35 ± 0.01	120 ± 3	28 ± 1	0.3 ± 0.04	−9.9 ± 0.1	5.65 ± 0.04	−3.7 ± 0.1
Q51A	1.36 ± 0.03	212 ± 20	47 ± 5	2.6 ± 0.2	−6.1 ± 0.3	7.6 ± 0.2	−0.2 ± 0.3
N61A	0.50 ± 0.01	44 ± 1	401 ± 10	1.8 ± 0.1	−18 ± 1	7.7 ± 0.1	−13 ± 1
Q99A	0.46 ± 0.02	13 ± 1	142 ± 10	−2.00 ± 0.04	−8.4 ± 0.3	4.67 ± 0.06	−3.1 ± 0.3
E110A	1.04 ± 0.02	48 ± 1	41 ± 1	2.1 ± 0.1	−10.8 ± 0.1	8.0 ± 0.1	−4.8 ± 0.1

[a] The Hill coefficient is related to the stepwise binding parameters as follows: $n_H = 2/[1 + (K_{d_2}^{obs}/K_{d_1}^{obs})^{1/2}]$. [b] Tochtrop et al. (2003) *Biochemistry 42*, 11561−11567. [c] This study.

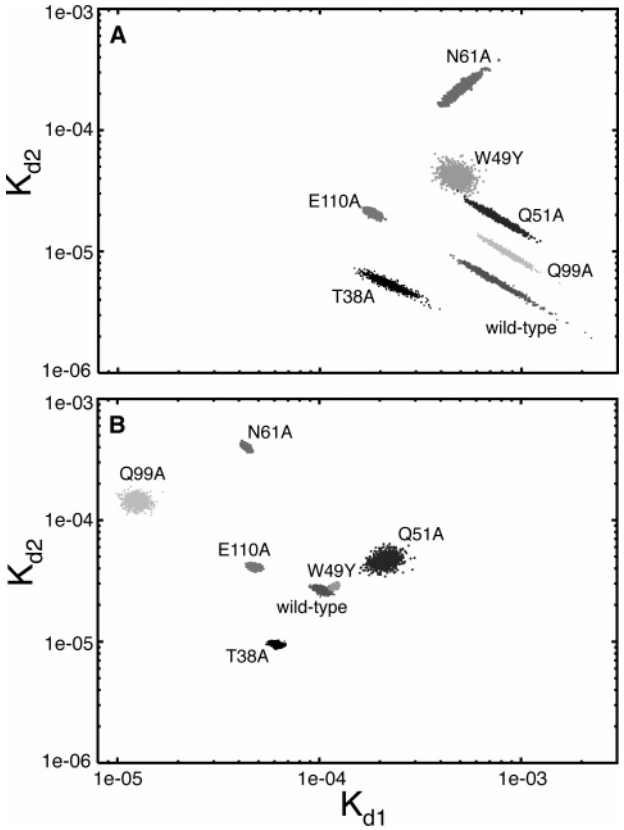

FIGURE 5: Bayesian analysis of the probability distribution for the fitted stepwise dissociation constants for GCA (A) and GCDA (B) binding to human I-BABP derivatives at 25 °C.

favorable contribution. This indicates the dominating role of the hydrophobic effect in the first binding step as bile salts are driven out of the water phase into the binding cavity of I-BABP. The second binding step, on the contrary, is accompanied by a highly favorable enthalpy and an unfavorable entropy change. The favorable enthalpic contributions reflect bile salt−amino acid interactions as well as, most likely, interactions of bile salt with bound water molecules within the binding cavity of the protein. The unfavorable entropic contribution likely results from an unfavorable organization of water molecules around the hydrophobic surfaces of bound bile salts within the cavity.

While in most compromised human I-BABP derivatives (E110A, W49Y, and Q99A), the loss in favorable enthalpic interactions is the dominating factor, in the case of N61A, the loss in cooperativity exclusively seems to arise from the unfavorable entropic contributions accompanying the second binding step. In mutations that preserved cooperativity in the binding of GCA, GCDA, or both (e.g., Q51A and T38A), favorable (unfavorable) enthalpic and unfavorable (favorable) entropic terms relative to the WT protein compensate each other (Tables 1 and 2).

^{15}N and ^{13}C NMR Experiments To Monitor Site Selectivity in Bile Acid Binding. To monitor the changes in the chemical environment of GCA and GCDA upon binding to various human I-BABP mutants, two-dimensional ^{15}N- and ^{13}C-heteronuclear single-quantum coherence (HSQC) spectra were collected on isotopically enriched bile salts complexed with mutant proteins. In one type of experiment, mutants were incubated with either ^{15}N-labeled GCA or ^{13}C-labeled GCDA in a 3:1 bile salt/protein ratio. In a second type of experiment, mutants were incubated with heterologous mixtures of the two bile salts in a 1.5:1.5:1 ^{15}N-labeled GCA/^{13}C-labeled GCDA/protein ratio. The position of the labels is shown in Figure 1.

Near room temperature, exchange broadening between bound and unbound peaks in the NMR spectra obscured the analysis of site specificity. NMR experiments were also complicated by the strong tendency of certain mutants to aggregate at concentrations practical for NMR data collection. To overcome these difficulties, experiments were performed at 10 °C. In the case of W49Y and Q51A, additional spectra were collected at 17 °C, which showed the same characteristics in binding site occupancy.

As we have shown earlier (*9*), when WT human I-BABP is incubated with only GCA or GCDA, both binding sites become occupied. However, when the protein is incubated with a mixture of the two bile salts, GCA binds nearly exclusively to site 2, while GCDA binds nearly exclusively to site 1.

Parts A−D in Figure 6 show contour plot representations of the^{15}N-HSQC spectra of ^{15}N-GCA complexed with WT, Q99A, Q51A, and N61A human I-BABP in a 3:1 molar ratio. Peak U represents unbound GCA, as assigned by otherwise identical control samples lacking protein. As we can see, similarly to the WT protein, both sites are occupied in each mutant protein. Parts E−H of Figure 6 display contour plot representations for samples containing a mixture of ^{15}N-GCA and ^{13}C-GCDA and the corresponding human I-BABP variant in a 1.5:1.5:1 molar ratio. In the case of Q99A and N61A, similarly to WT human I-BABP, the presence of GCDA results in the loss of the resonance corresponding to GCA bound to site 1. Similar behavior was found for mutants T38A, W49Y, and E110A (data not shown). In the case of Q51A (parts C and G of Figure 6), both binding sites remained occupied by GCA, despite the presence of an

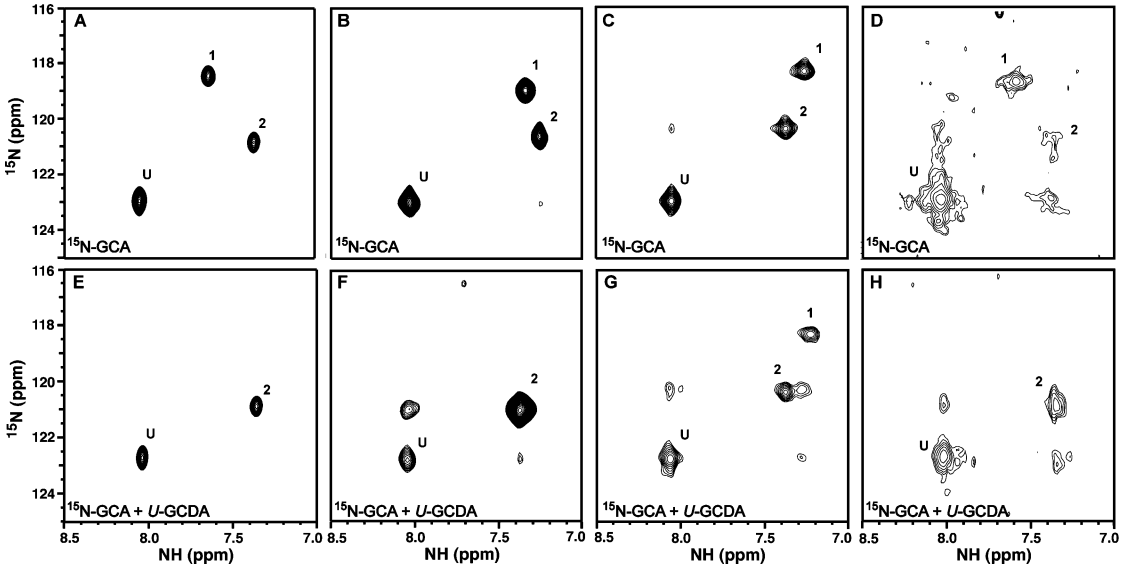

FIGURE 6: Contour plot representations (U, unbound bile salt; 1, bile salt bound to site 1; 2, bile salt bound to site 2) of gradient- and sensitivity-enhanced ^{1}H/^{15}N-HSQC spectra of ^{15}N-labeled GCA for a sample containing [^{15}N]GCA/WT hI-BABP (A), [^{15}N]GCA/Q99A hI-BABP (B), [^{15}N]GCA/Q51A hI-BABP (C), and [^{15}N]GCA/N61A hI-BABP (D) in a 3:1 molar ratio. Contour plot representations of ^{15}N-HSQC spectra of ^{15}N-labeled GCA for a sample containing [^{15}N]GCA/[1′,2′]-$^{13}C_2$-GCDA/WT hI-BABP (E), [^{15}N]GCA/[1′,2′]-$^{13}C_2$-GCDA/Q99A hI-BABP (F), [^{15}N]GCA/[1′,2′]-$^{13}C_2$-GCDA/Q51A hI-BABP (G), and [^{15}N]GCA/[1′,2′]-$^{13}C_2$-GCDA/N61A hI-BABP (H) in a 1.5:1.5:1 molar ratio.

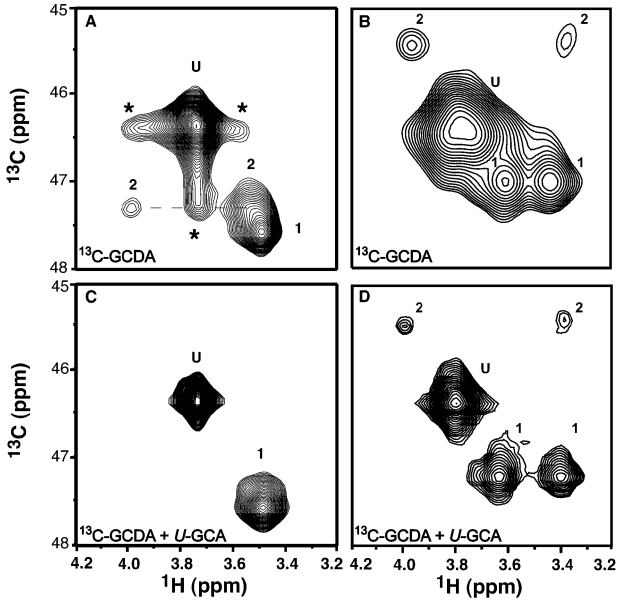

FIGURE 7: Contour plot representations (U, unbound bile salt; 1, bile salt bound to site 1; 2, bile salt bound to site 2) of gradient-enhanced ^{1}H/^{13}C-HSQC spectra of [1′,2′]-$^{13}C_2$-GCDA for a sample containing [1′,2′]-$^{13}C_2$-GCDA/WT hI-BABP (A), [1′,2′]-$^{13}C_2$-GCDA/Q51A hI-BABP (B), [^{15}N]GCA/[1′,2′]-$^{13}C_2$-GCDA/WT hI-BABP (C), [^{15}N]GCA/[1′,2′]-$^{13}C_2$-GCDA/Q51A hI-BABP (D). The bile salt/protein molar ratios were 3:1 for A and B and 1.5:1.5:1 for C and D.

equimolar amount of GCDA. Thus, unlike in WT human I-BABP and the rest of the engineered mutations, in Q51A, ^{13}C-GCDA was not able to displace ^{15}N-GCA from site 1.

To determine whether the mutation at Q51 resulted in the loss of site discrimination for GCA also, ^{13}C-HSQC spectra of ^{13}C-GCDA bound to Q51A human I-BABP were collected in both the absence and presence of an equimolar amount of ^{15}N-GCA (parts B and D of Figure 7). Unlike in the case of the WT protein (parts A and C of Figure 7) and the rest of the investigated mutations, GCA was not able to displace GCDA from site 2. Thus, the mutation at Q51 resulted in the loss of site preference for both bile salts.

A comparison of the ^{15}N- and ^{13}C-HSQC spectra of labeled bile salts bound to WT and various mutant I-BABP derivatives reveals significant differences in chemical shifts for almost each mutant, indicating changes in the chemical environment of bile salt side chains compared to the WT protein. The largest changes occur for Q51A and Q99A. In the case of Q51A, the ^{1}HN resonance of ^{15}N-GCA bound to site 1 as well as the $^{13}C_\alpha$ resonance of ^{13}C-GCDA bound to site 2 are both shifted upfield (to smaller frequencies) by approximately 0.4 and 2 ppm, respectively. In the heterotypic complex, we also notice an upfield shoulder for the amide resonance of GCA bound to site 2. This may be an indication of two slightly different populations of GCA at site 2, particularly, that we also see an exchange peak between this shoulder and unbound GCA (Figure 6G).

For Q99A, the ^{1}HN resonance of ^{15}N GCA bound to site 1 is shifted upfield by approximately 0.3 ppm, and the $^{13}C_\alpha$ resonance of ^{13}C-labeled GCDA bound to site 1 is shifted downfield (to higher frequencies) by 1.5 ppm. For this mutant, we also see a significant chemical-shift difference between the homotypic and heterotypic complexes: in the presence of both GCA and GCDA, the ^{15}N and ^{1}HN resonances of GCA bound to site 2 move to higher frequencies by approximately 0.7 and 0.1 ppm (parts B and F of Figure 6). If this would arise from chemical exchange of GCA between sites 1 and 2, the shift in the heterotypic complex would fall between the shifts for site 1 and 2 in the homotypic complex. Because this is not the case, the observed differences in the chemical shifts must reflect changes in the chemical environment of the glycine moiety of GCA depending upon whether GCDA is also present in the binding pocket.

Bile salt peaks are severely broadened in the complex of N61A, the I-BABP mutant in which the binding energetics was most severely compromised (parts D and H of Figure

6). The presence of exchange peaks in the spectra indicates that the loss of signal intensity arises from chemical exchange between the bound and unbound states. The faster off rate of GCA is supported by the ITC data that shows more than an order of magnitude decrease in the overall binding affinity of N61A for GCA compared to WT human I-BABP. In the heterotypic complex of N61A (Figure 6H), the exchange broadening is somewhat reduced. In the case of Q99A and Q51A, on the other hand, we see increased exchange between bound and unbound GCA when the other site is occupied by GCDA (parts F and G of Figure 6). The existence of exchange peaks suggests that, although the bound and unbound populations of bile salts are in slow exchange on the chemical-shift time scale (there are distinct peaks for bound and unbound ligands), the exchange rate between unbound GCA and GCA bound at site 2 is approaching the faster end of this time scale (milli- to subseconds). A similar exchange broadening is observed for GCDA in WT protein between unbound GCDA and GCDA bound at site 2 (Figure 7A).

Mutant Q51A displays large differences in the intensity of ^{13}C-GCDA bound at sites 1 and 2 (parts B and D of Figure 7). Nevertheless, the population of GCDA bound at site 1 cannot be dismissed. The intensity differences are in fact comparable to those observed in the WT complex. This becomes more apparent when we consider that, in the spectra of ^{13}C-GCDA complexed with WT protein, there is an overlap between one of the α protons of GCDA bound at site 2 and the α protons of GCDA bound at site 1 (large asymmetric peak at 3.5 and 47.5 ppm in Figure 7A). The other α proton of GCDA bound at site 2 is well-resolved at 3.94 and 47.4 ppm. Its intensity is much less than a third of the intensity of the overlapped peak at 3.5 and 47.5 ppm thus has to be well below the intensity of GCDA bound at site 1 as well. We observed similar intensity differences between sites 1 and 2 in the ^{15}N-HSQC spectrum of ^{15}N-GCDA and in the 2D HCACO spectrum of ^{13}C-GCDA complexed with WT protein (data not shown). The intensity differences arise from differences in the intrinsic affinities of GCDA for sites 1 and 2. This is a markedly different binding characteristic from GCA (*9*), which we believe plays a significant role in site selectivity in the heterotypic complex.

In WT human I-BABP, GCDA displays a distinct behavior in the sense that at site 2 the α-carbon protons display a diastereotopic doublet [indicating a unique chemical environment that is in slow exchange on the NMR time scale (∼10 ms) for each geminal proton], whereas at site 1, they appear as a singlet (suggesting free rotation for the glycine side chain on the NMR time scale). Among the engineered mutations, only Q99A and T38A displayed the same behavior. For all other investigated mutations, the geminal protons of the α carbon of GCDA appeared to be in distinct chemical environments when bound to site 1, suggesting that the glycine side chain was rigidly anchored to the protein.

Protein Stability. The stability of WT and mutant human I-BABP proteins was determined by urea-induced changes in intrinsic tryptophan (WT, T38A, Q51A, N61A, Q99A, and E110A) or tyrosine (W49Y) fluorescence. The midpoints of the denaturation curves ranged between 1.6 and 3.4 M, with E110A being the least stable mutant (Table 3). Free-energy changes of unfolding at a 0 urea concentration ranged between 2.6 and 6.2 kcal/mol. Interestingly, among the proteins that were produced as inclusion bodies (T38A, N61A, and E110A), only E110A showed significantly diminished stability from the WT protein. A comparison of mutant−WT differences in free-energy changes of denaturation to mutant−WT differences in free-energy changes accompanying bile salt binding shows no correlation. The lack of correlation between the two is an indication that the changes that we observed in binding cooperativity are not consequences of inherent changes in protein stability but rather reflections of subtle changes in the communication pathway between the two binding sites. A similar lack of correlation between stability and binding affinity was reported earlier for adipocyte and intestinal fatty-acid-binding proteins (*35*).

Table 3: Stability of Human I-BABP Derivatives Determined by Urea Denaturation at 25 °C

hI-BABP type	$[D]_{50\%}$[a]	m[b]	ΔG[c]
wild type	3.40 ± 0.16	−1.78 ± 0.01	5.9 ± 0.1
T38A	2.32 ± 0.03	−2.04 ± 0.12	4.7 ± 0.2
W49Y	2.66 ± 0.09	−1.75 ± 0.03	4.7 ± 0.3
Q51A	3.39 ± 0.13	−1.66 ± 0.17	5.6 ± 0.4
N61A	2.63 ± 0.06	−1.77 ± 0.02	4.7 ± 0.1
Q99A	3.14 ± 0.06	−1.96 ± 0.04	6.2 ± 0.3
E110A	1.63 ± 0.20	−1.62 ± 0.22	2.6 ± 0.1

[a] The urea concentration (M) at which the Trp fluorescence is reduced by 50%. [b] The slope [kcal/(mol M)] of the variation of ΔG with the urea concentration. [c] The free energy of unfolding (kcal/mol) at 0 M urea concentration.

Table 4: Effect of Mutations on Binding Cooperativity and Site Selectivity

little or no effect on cooperativity	loss of positive cooperativity	mixed effect on cooperativity
	N61A	W49Y
T38A	GCA, partial loss	GCA, partial loss
	GCDA, complete loss	GCDA, no effect
	E110A	Q99A
Q51A	GCA, partial loss	GCA, no effect
	GCDA, complete loss	GCDA, complete loss

little or no effect on site selectivity	loss of site selectivity
T38A W49Y N61A Q99A E110A	Q51A

DISCUSSION

In the context of binding cooperativity and site selectivity, the investigated human I-BABP mutations can be grouped into four distinct categories (Table 4): (1) mutations that compromised positive cooperativity in the binding of both GCA and GCDA (N61A and E110A), (2) mutations that compromised positive cooperativity in the binding of either GCA (W49Y) or GCDA (Q99A), (3) a mutation that compromised site selectivity in bile salt human I-BABP recognition (Q51A), and finally, (4) a mutation that did not affect either binding cooperativity or site selectivity within the margin of experimental error (T38A). None of the mutations that resulted in diminished binding cooperativity showed any substantial loss in site selectivity, and the only mutation that resulted in the loss of site selectivity exhibited no decrease in binding cooperativity.

Given the fact that at 20 °C the intrinsic affinities of GCA for sites 1 and 2 are nearly identical (*7*), we initially hypothesized that the site selectivity of GCA in the heterotypic system arises from differences in cooperativity (*7*). In other words, it seemed plausible that binding of GCA to site 2 involves specific interactions with the protein that lead to an energetic communication that enhances the binding to the other site, an effect that GCA might not be able to exert through its interaction with site 1.

Because we previously observed an increase in macroscopic cooperativity in GCA binding with decreasing temperatures, it is likely that, at temperatures that the NMR experiments were carried out, cooperativities in both GCA and GCDA binding were somewhat higher than those reported by ITC at 25 °C. Nevertheless, the fact that we have not observed any sign of correlation between losses in macroscopic binding cooperativity and losses in site selectivity indicates that the two phenomena are not linked as closely as suggested by the intrinsic binding affinities of GCA.

A comparison of the stepwise dissociation constants for GCA and GCDA in the WT protein reveals an apparent 7-fold stronger first binding step for GCDA. Despite the diminished positive cooperativity in GCDA binding, the increased strength of the first step leads to an approximately 2-fold increase in the overall binding affinity for GCDA relative to GCA. Using specifically ^{13}C- and ^{15}N-labeled GCDA and the same type of NMR assay that we developed in our laboratory for GCA (*7*), we attempted the determination of site-specific binding constants for GCDA as well but strong exchange broadening between bound and unbound peaks obscured the spectra even at 10 °C. Nevertheless, the stronger intrinsic affinity of GCDA for site 1 is well-established by the combination of two results: (i) a stronger overall affinity but reduced positive-binding cooperativity relative to GCA and (ii) a preference of GCDA for site 1 in the heterotypic WT complex. These observations and the lack of correlation between cooperativity and site selectivity revealed by the mutagenesis study all point toward the likely explanation that site selectivity in the heterotypic complex of human I-BABP is in fact from the increased intrinsic affinity of GCDA for site 1. This notion is further supported by two additional findings: (i) in Q51A, the I-BABP mutant in which we abolished site selectivity, the overall binding affinity for GCDA is about 4 times weaker than in WT protein, while (ii) for WT I-BABP, the overall enthalpic contribution to the free-energy change upon GCDA binding is above 70% and, for Q51A, it is only 30%.

On the basis of the first generation NMR structure of the ternary complex and the mutagenesis results, we envision two cooperativity networks in the doubly ligated system: an upper network that involves the steroid ring hydroxyl group at position C-12 (present only in GCA) and a lower network that involves the steroid ring hydroxyl groups at positions C-3 and C-7 (present in both GCA and GCDA) (Figure 2B).

Among the investigated mutations, N61A is the most severely compromised mutant. In addition to the dramatic loss of cooperativity in its interaction with both GCA and GCDA, it has a severely diminished overall binding affinity for both bile salts. According to our first generation NMR structure of the ternary complex, N61 is located on β-strand D near site 1 in the vicinity of the steroid ring hydroxyl groups at positions C-7 and C-12 (Figure 2). The dramatic effect of the mutation at N61 on the binding energetics and the unique location of the asparagine side chain suggests that N61 serves as a specific anchor at site 1 that positions the steroid ring system of the bound bile salt appropriately so that it could most effectively participate in additional interactions that are part of either the upper or lower communication pathway between the two sites. These additional interactions most likely include residues W49, E110, and possibly Q99.

The bulky side chain of W49 is located in the center of the binding pocket offering not only hydrogen-bonding but also extensive hydrophobic interactions with the ligands at both sites. Because mutant W49Y compromises only the cooperativity in GCA binding (the same is observed for W49F, data not shown), it is likely that this residue is a member of the upper communication network, the one that includes the steroid ring hydroxyl group at position C-12.

In contrast, mutation at E110 diminishes cooperativity in both GCA and GCDA binding, indicating a 3-OH and/or a 7-OH connection. This is also supported by the first generation NMR structure of the ternary complex: the side chain of E110 appears to be within hydrogen-bonding distance to the 7-OH of GCA at site 2 and in proximity to the 3-OH of the bound bile salt at site 1. Thus, the glutamate side chain of E110 is likely part of the lower cooperativity network that includes the steroid ring hydroxyl groups at positions C-3 and C-7.

Interestingly, while the mutation at Q99 results in a dramatic loss of binding cooperativity for GCDA, it has no effect on the binding properties of GCA. If Q99 would be part of the lower cooperativity network, it should have at least some effect on the binding cooperativity of GCA as well. Because this is not the case, we believe that the differences in the binding energetics of GCDA that we observe between Q99A and WT human I-BABP are manifestations of different intrinsic affinities of the bile salt for site 1 in the two proteins.

Similarly to N61, the side chain of Q99 is located near site 1, in proximity to the steroid ring hydroxyl group at position C-7. Changing the glutamine or asparagine side chain to a methyl group not only disrupts the hydrogen-bonding communication pathway between the two sites but also changes the polarity of the binding pocket. On the basis of the appearance of the NMR spectra and the relations of K_{d_1} and K_{d_2}, site 1 is still preferred over site 2 by GCDA in both Q99A and N61A. The negative cooperativity exhibited by these mutants suggests that the positioning of GCDA at site 1 is not ideal for a second ligand to bind at site 2.

The unique characteristics of positive-binding cooperativity and site selectivity in human I-BABP have implications for its biological function. In the human body, approximately 55% of bile salts have three and approximately 35% of bile salts have two hydroxyl groups on their steroid ring system. For a doubly ligated complex with two different ligands, there are four possible ligation states. In the ternary complex of I-BABP with GCA and GCDA, these possibilities would be (i) GCA at both sites, (ii) GCDA at both sites, (iii) GCA at site 1 and GCDA at site 2, and (iv) GCDA at site 1 and GCA at site 2. In the absence of site selectivity, the highly cooperative homotypic GCA complexes would be energetically favored and nature would need to develop a different bile salt binding protein to recognize dihydroxy bile salts.

Thus, on one hand, site selectivity ensures that the majority of I-BABP complexes *in vivo* are heterotypic: they contain both dihydroxy and trihydroxy bile salts. On the other hand, we previously reported that, when both bile salts are bound, the strength of positive cooperativity appears to be the average of the cooperativities observed in the homotypic complexes (*8*). Therefore, although dihydroxy bile salts exhibit only modest positive cooperativity, heterotypic complexes will still maintain a high degree of positive cooperativity. In combination with the relatively low intrinsic affinities of I-BABP for both GCA and GCDA, this allows a sizable fraction of bile salts to remain unbound at a low bile salt concentration (passing through the enterocytes as monomers) whereas protecting the cells from bile salt toxicity (e.g., apoptosis) at high bile salt concentrations. Thus, with the combination of site selectivity and positive-binding cooperativity, nature engineered human I-BABP to be a highly efficient regulator that is able to recognize structurally diverse bile salts that exist in the human body.

In conclusion, the investigation of six single-point mutations in the binding cavity of human I-BABP suggests that cooperativity and site selectivity are not linked in the protein. While cooperativity in bile salt binding is the result of a subtle interplay of entropic and enthalpic contributions, site selectivity appears to be determined by more localized enthalpic effects. More specifically, site-directed mutagenesis and previous thermodynamic characterization of bile salt binding to human I-BABP indicate that the strong intrinsic affinity of GCDA for site 1 plays a key role in the site selectivity of bile salt binding. We are currently solving the 3D NMR structure of the WT and a mutant I-BABP protein. The comparison of the two should give us further insights into the structural correlates of cooperativity and site selectivity in human I-BABP.

ACKNOWLEDGMENT

This work was supported by USPHS NIH Grant R01 DK48046 to D.P.C. and by the Washington University Digestive Diseases Research Core Center, USPHFS NIH Grant P30 DK52574.

REFERENCES

1. Veerkamp, J. H., and Maatman, R. G. (1995) Cytoplasmic fatty acid-binding proteins: Their structure and genes, *Prog. Lipid Res. 34*, 17−52.
2. Glatz, J. F., and van der Vusse, G. J. (1996) Cellular fatty acid-binding proteins: Their function and physiological significance, *Prog. Lipid Res. 35*, 243−282.
3. Lin, M. C., Kramer, W., and Wilson, F. A. (1990) Identification of cytosolic and microsomal bile acid-binding proteins in rat ileal enterocytes, *J. Biol. Chem. 265*, 14986−14995.
4. Sacchettini, J. C., Hauft, S. M., van Camp, S. L., Cistola, D. P., and Gordon, J. I. (1990) Developmental and structural studies of an intracellular lipid binding protein expressed in the ileal epithelium, *J. Biol. Chem. 265*, 19199−19207.
5. Miller, K. R., and Cistola, D. P. (1993) Titration calorimetry as a binding assay for lipid-binding proteins, *Mol. Cell. Biochem. 123*, 29−37.
6. Small, D. M., Dowling, R. H., and Redinger, R. N. (1972) The enterohepatic circulation of bile salts, *Arch. Intern. Med. 130*, 552−573.
7. Tochtrop, G. P., Richter, K., Tang, C., Toner, J. J., Covey, D. F., and Cistola, D. P. (2002) Energetics by NMR: Site-specific binding in a positively cooperative system, *Proc. Natl. Acad. Sci. U.S.A. 99*, 1847−1852.
8. Tochtrop, G. P., Bruns, J. M., Tang, C., Covey, D. F, and Cistola, D. P. (2003) Steroid ring hydroxylation patterns govern cooperativity in human bile acid binding protein, *Biochemistry 42*, 11561−11567.
9. Tochtrop, G. P., DeKoster, G. T., Covey, D. F., and Cistola, D. P. (2004) A single hydroxyl group governs ligand site selectivity in human ileal bile acid binding protein, *J. Am. Chem. Soc. 126*, 11024−11029.
10. Higuchi, R., Krummel, B., and Saiki, R. K. (1988) A general method of *in vitro* preparation and specific mutagenesis of DNA fragments: Study of protein and DNA interactions, *Nucleic Acid Res. 16*, 7351−7367.
11. Ho, S. N., Hunt, H. D., Horton, R. D., Pullen, J. K., and Pease, L. R. (1989) Site-directed mutagenesis by overlap extension using the polymerase chain reaction, *Gene 77*, 51−59.
12. Hodsdon, M. E., Toner, J. J., and Cistola, D. P. (1995) ^{1}H, ^{13}C, and ^{15}N assignments and chemical shift-derived secondary structure of intestinal fatty acid-binding protein, *J. Biomol. NMR 6*, 198−210.
13. Johnson, B. H., and Hecht, M. H. (1994) Recombinant proteins can be isolated from *E. coli* cells by repeated cycles of freezing and thawing, *Biotechnology 12*, 1357−1360.
14. Pace, C. N., Vajdos, F., Fee, L., Grimsley, G., and Gray, T. (1995) How to measure and predict the molar absorption coefficient of a protein, *Protein Sci. 4*, 2411−2423.
15. Tserng, K. Y., Hachey, D. L., and Klein, P. D. (1977) An improved procedure for the synthesis of glycine and taurine conjugates of bile salts, *J. Lipid Res. 18*, 404−407.
16. Wittekind, M., and Mueller, L. (1993) HNCACB, a high sensitivity 3D NMR experiment to correlate amide-proton and nitrogen resonances with the α- and β-carbon resonances in proteins, *J. Magn. Res. B 101*, 201−205.
17. Muhindaram, D. R., and Kay, L. E. (1994) Gradient-enhanced triple-resonance three-dimensional NMR experiments with improved sensitivity, *J. Magn. Res. B 103*, 203-216.
18. Kay, L. E., Xu, G. Y., and Yamazaki, T. (1994) Enhanced-sensitivity triple-resonance spectroscopy with minimal H_2O saturation, *J. Magn. Res. A 109*, 1290−133.
19. Grzesiek, S., and Bax, A. (1992) Correlating backbone amide and side chain resonances in larger proteins by multiple relayed triple resonance NMR, *J. Am. Chem. Soc. 114*, 6291−6293.
20. Ikura, M., Kay, L. E., and Bax, A. (1990) A novel approach for sequential assignment of proton, carbon-13, and nitrogen-15 spectra of larger proteins: Heteronuclear triple-resonance three-dimensional NMR spectroscopy. Application to calmodulin, *Biochemistry 29*, 4659−4667.
21. Grzesiek, S., and Bax, A. (1992) Improved 3D triple-resonance NMR techniques applied to a 31 kDa protein, *J. Magn. Res. 96*, 432−440.
22. Kay, L. E. (1993) Pulsed-field gradient-enhanced three-dimensional NMR experiment for correlating ^{13}Cα/β, ^{13}C′, and ^{1}Hα chemical shifts in uniformly carbon-13-labeled proteins dissolved in water, *J. Am. Chem. Soc. 115*, 2055−2057.
23. Grzesiek, S., Anglister, J., and Bax, A. (1993) Correlation of backbone amide and aliphatic side-chain resonances in ^{13}C/^{15}N-enriched proteins by isotropic mixing of ^{13}C magnetization, *J. Magn. Res. 101*, 114−119.
24. Kay, L. E., Xu, G. Y., Singer, A. U., Muhandiram, D. R., and Forman-Kay, J. D. (1993) A gradient enhanced HCCH-TOCSY experiment for recording side-chain proton and carbon-13 correlations in water samples of proteins, *J. Magn. Res. B 101*, 333−337.
25. Prompers, J. J., Groenewegen, A., Hilbers, C. W., and Pepermans, H. A. M. (1998) Two-dimensional NMR experiments for the assignment of aromatic side chains in ^{13}C-labeled proteins, *J. Magn. Res. 130*, 68−75.
26. Clore, G. M., Kay, L. E., Bax, A., and Gronenborn, A. M. (1991) Four-dimensional ^{13}C/^{13}C-edited nuclear Overhauser enhancement spectroscopy of a protein in solution: Application to interleukin 1 β, *Biochemistry 30*, 12−18.
27. Zhang, O., Forman-Kay, J. D., Shortle, D., and Kay, L. E. (1997) Triple-resonance NOESY-based experiments with improved spectral resolution: Applications to structural characterization of unfolded, partially folded and folded proteins, *J. Biomol. NMR 9*, 181−200.
28. Kay, L. E., Keifer, P., and Saarinen, T. (1992) Pure absorption gradient enhanced heteronuclear single quantum correlation spectroscopy with improved sensitivity, *J. Am. Chem. Soc. 114*, 10663−10665.

29. John, B. K., Plant, D., Webb, P., and Hurd, R. E. (1992) Effective combination of gradients and crafted RF pulses for water suppression in biological samples, *J. Magn. Res. 98*, 200−206.
30. Wishart, D. S., and Sykes, B. D. (1994) The ^{13}C chemical shift index: A simple method for the identification of protein secondary structure using chemical shift data, *J. Biomol. NMR 4*, 171−180.
31. Lücke, C., Zhang, F., Hamilton, J. A., Sacchettini, J. C., and Rüterjans, H. (2000) Solution structure of ileal lipid binding protein in complex with glycocholate, *Eur. J. Biochem. 267*, 2929−2938.
32. Warren, J. R., and Gordon, J. A. (1966) On the refractive indices of aqueous solutions of urea, *J. Phys. Chem. 70*, 297−300.
33. Santoro, M. M., and Bolen, D. W. (1988) Unfolding free energy changes determined by the linear extrapolation method. 1. Unfolding of phenylmethane-sulfonyl-α-shymotrypsin using different denaturants, *Biochemistry 27*, 8063−8068.
34. Berry, D. A. (1996) *Statistics: A Bayesian Perspective*, Duxbury Press, Belmont, CA.
35. Richieri, G. V., Low, P. J., Ogata, R. T., and Kleinfeld, A. M. (1998) Thermodynamics of fatty acid binding to engineered mutants of the adipocyte and intestinal fatty acid-binding proteins, *J. Biol. Chem. 273*, 7397−7405.

BI051781P